MeV ion implantation for modification of electronic, optical, and magnetic materials

S. Roorda, F. Schiettekatte, M. Cai, T. Veres, and A. Tchebotareva.

Département de physique et Groupe de recherche en physique et technologie des couches minces, Université de Montréal, CP 6128 succursale Centre-ville, Montréal H3C 3J7 Canada

ABSTRACT

The University of Montreal recently inaugurated a new 1.7 MV Tandem accelerator for materials research. It is being used to study a wide range of topics involving optical, electronic, opto-electronic, and magnetic materials. Current research includes: threshold dose for secondary damage in Si, gettering of impurities in Si by nano-cavities, ion beam mixing of metallic multilayers probed by giant magnetoresistance, tracks and deformations induced by multi-MeV ion beams, and high-resolution radial distribution function of pure amorphous silicon. A selection of recent results is discussed.

Keywords: ion implantation, optical materials, amorphous materials, magnetic materials, electronic materials

1. INTRODUCTION

Ion implantation is virtually the only technique used today to achieve electrical doping in selected areas of silicon wafers during microelectronic device manufacturing, and as such it is a well established and well understood process[1]. This is in large part due to the excellent effective and independent control it offers over different aspects of the required doping, such as species, depth, and doping concentration, and in much smaller part due to the highly non-equilibrium nature of the process. From a research point of view, it is the latter aspect that offers the greatest potential, and at the same time the greatest challenge. Because of its highly non-equilibrium character, ion beam modification with MeV ions offers unique opportunities for new processing and new understanding of a range of materials much broader than only the semiconductors. With this in mind, the University of Montreal recently acquired a new MeV Tandem accelerator, capable of accelerating a wide selection of ions over a wide range of energies. As a note of interest, this accelerator is housed under the same roof as the prototype of all Tandems, the 6 MV HVEE EN-1 Tandem accelerator that was constructed in 1957 and 1958 for Chalk River Research Laboratories, and is still functional today. The new machine has now been operational for a little more than one year, and some of the subjects being studied using either the old or the new accelerator are discussed in these proceedings.

2. 1.7 MV TANDEM ACCELERATOR

For those working in the field of MeV ion implantation, tandem accelerators are recognized as versatile workhorses. Multiple ion sources can be mounted at the same time, which allows for rapid turnover times between different ion beams. Moreover, these ion sources are located outside of the (SF_6) pressurized HV vessel and therefore easily accessible for fine-tuning and maintenance. The ion sources should deliver negative ions that are accelerated towards the high voltage terminal inside the HV vessel, stripped of two or more electrons, and accelerated a second time by the same high voltage (whence the name Tandem accelerator) but now away from the high voltage terminal. The Montréal Tandetron, manufactured by High Voltage Engineering Europe BV, is equipped with two ion sources (see Fig. 1). One ion source is a duoplasmatron source which is used exclusively for He ions, the only noble gas that forms a stable negative ion, and the other is a Cs sputter ion source which is used for all other elements. The negative ions are not pre-accelerated after having been extracted from the ion sources, which greatly simplifies the layout of the injector stage of the accelerator.

The accelerating voltage can be varied from 50 kV to 1.7 MV, which corresponds with a minimum acceleration of 100 keV (for singly charged ions) to 5.1 MeV (for singly charged negative ions in and double positively charged ions out). However, for low acceleration potentials (< 200 kV), the electron stripping action becomes inefficient and only small ion beam current can be obtained (typically less than a few μA, compared to more than 100 μA for some ions at full accelerating potential).

Part of the SPIE Conference on Materials Modification by Ion Irradiation • Québec, Canada • July 1998
SPIE Vol. 3413 • 0277-786X/98/$10.00

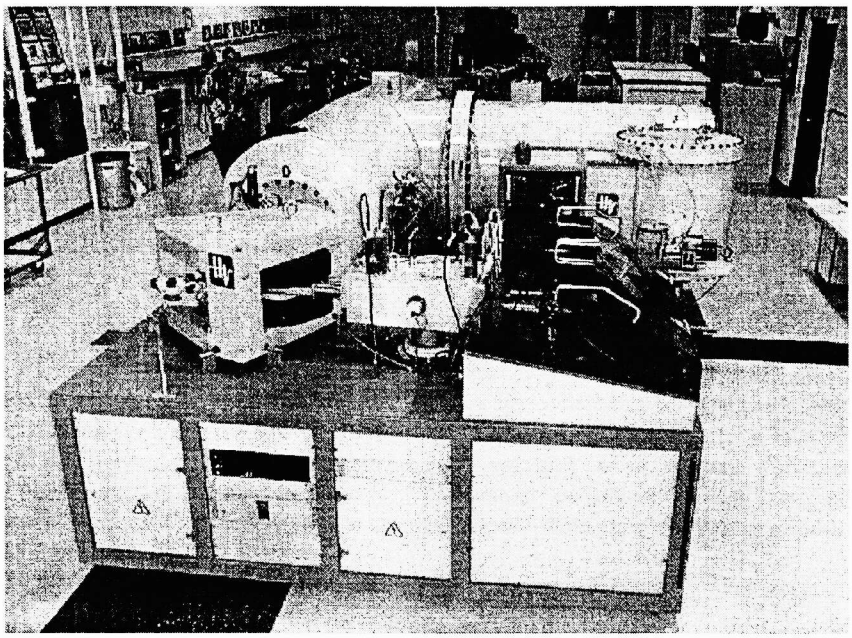

Figure 1. Photograph of the injector stage of the Tandetron accelerator. The two large dark covers on the right side providing isolation from the extraction voltage hide the ion sources. The extracted ions are mass analyzed by a 90° bending magnet. Behind the injector stage the HV vessel is visible. The large structure perpendicular to the acceleration direction houses the high voltage generator.

This is in spite of the fact that the (gas) stripping is much improved over older gas strippers by using a turbo-molecular pump which recirculates the stripper gas that leaks out of the stripper back into the stripper canal. Use of a recirculator allows larger diameter stripping canal and high stripper gas pressures to be used, while minimizing the residual pressure of leaked stripper gas along the accelerator columns. The reduced gas leakage, together with inclined field accelerator tubes and a modest amount of lead shielding on the HV vessel are also very effective at suppressing brehmsstrahlung normally associated with MeV accelerators, to levels well below the 2.5 μSv/hr (0.25 mR/hr) exposure limit for the general public.

A combined analysis and switching magnet is employed to select only one of the charge states (and whence energies) of the accelerated ion beam and to send it down one of two beam lines (see Figure 2). One beam line (at minus 30°) is equipped with a scattering chamber for Rutherford back-scattering spectroscopy (RBS) and channeling, the other beam line is equipped for ion implantation. The implantation line consist of, in downstream sequence: slits, a removable beam stop/Faraday cup, an electrostatic raster scanner, an electrostatic deflector, a vacuum valve, an exchangeable aperture, an exchangeable sample holder, and an end beam stop/Faraday cup. Most of these items are standard beam line components but since their functionality can affect the results of an ion implantation experiment in sometimes-unexpected ways, it seems appropriate to discuss a few aspects of the components in some detail.

For most experiments involving ion implantation, it is essential that the area to be implanted is well defined and laterally homogeneous. This is achieved with the raster scanner and the aperture (much like spraying paint through a stencil). The raster scanner employs horizontal and vertical scanning at two different frequencies (34 and 412 Hz) derived from a single quartz oscillator. The scan frequencies are chosen such that non-random variations in the ion beam intensity such as those caused by 50 or 60 Hz oscillations of the electrical power derived from the grid do not lead to inhomogeneities in the implanted region. By scanning over a region that is as least as wide and as high as the size of the aperture plus twice the width of the ion beam, the surface of the sample behind the aperture is either implanted with the foreseen areal dose, or not at all, *i.e.* edge effects are minimized. The electrostatic deflector serves to reject neutral atoms. (Some neutralization occurs as the ions travel through the vacuum system. Once the ions have been raster scanned that doesn't pose a problem but without the deflector, the neutral atoms passing through the raster scanner would hit the sample in a single spot in the middle of the scanned area.)

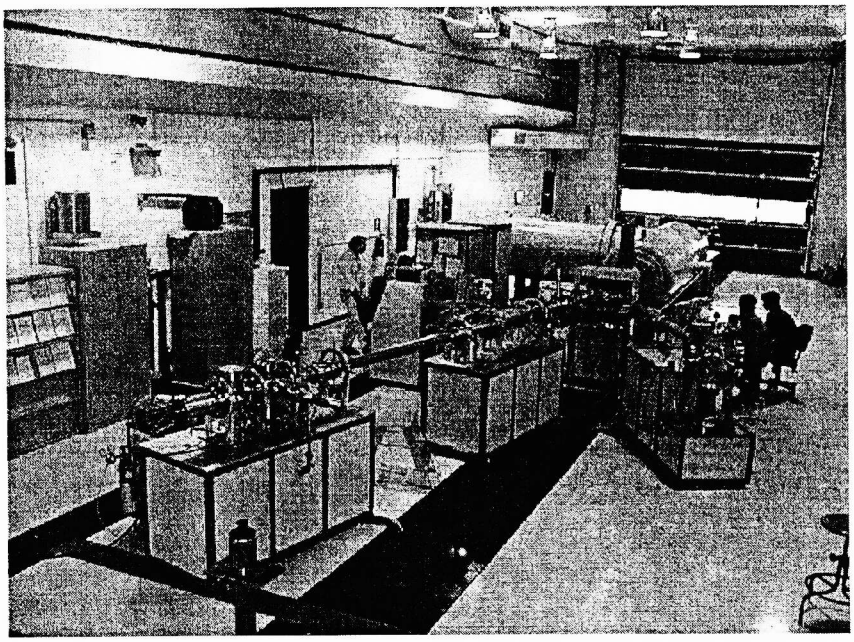

Figure 2. Photograph of the beam lines installed on the Tandetron accelerator. The short line on the right is the RBS/channeling line. The longer line on the left was build in-house and is the implantation line. The cabinet under the implantation line closest tot he switching magnet holds the power supplies for the raster scanner (itself visible in the beam line) and deflector, and the second cabinet holds the vacuum pumps for the implantation chamber.

The sample holder constitutes also an essential part of the ion implantation line, which merits a brief discussion. An ion beam of 10 μA (or 20 μA for doubly charged ions) at 5 MeV scanned over a 1 cm^2 area deposits 50 W/cm^2! Clearly massive cooling is required to keep the samples at a reasonable temperature. This is achieved by using a large copper block as sample holder, which provides a large thermal mass for improved temperature stability. Furthermore, the block is hollow and can be air cooled, filled with liquid nitrogen for deep cooling, or heated for hot or controlled temperature implantations. The copper block is electrically isolated from the flange used to mount it on the vacuum chamber so that the ion current during the implantation can be monitored. The implantation chamber is equipped with a screen around the copper sample holder, which is biased at –500 V to repel secondary electrons emitted from the sample; this makes that the integrated ion current is a reliable measure for the implantation dose.

3. TEMPERATURE DEPENDENCE OF THE CRITICAL DOSE FOR SECONDARY DEFECTS

The first -preliminary- result to be discussed is the temperature dependence of the critical dose for secondary defect formation. Ion implantation for doping in crystalline silicon inevitably creates lattice damage, and most of these point defects annihilate immediately during the implantation. Those that do not annihilate are normally removed by thermal anneals. However, if the lattice damage is quite extensive, then the annealing treatment cannot restore the original crystal structure and instead, secondary defects such as dislocation loops may form[2]. It has been shown that a well-defined critical ion dose exist which, if exceeded, leads to the formation of such secondary defects[3]. In fact, this dose is different for different ion species and energies but always amounts to the same areal defect density resulting from the implantation. However, repeated ion implantations, each followed by appropriate anneals, can be used to exceed the threshold without creating the secondary damage. This immediately raises the question of the influence of the target temperature during the ion implantation on this threshold. After all, the combination of beam flux and target temperature during the implantation establishes a certain steady state point defect concentration and this steady state level determines to some extent the amount of non-annealed damage at the end of the implantation.

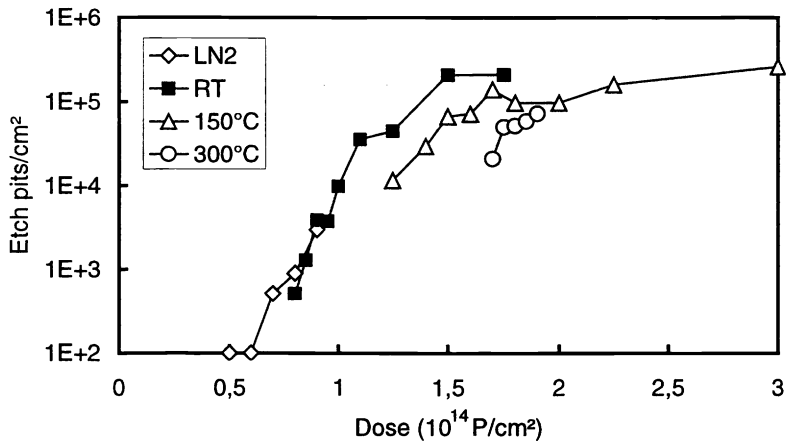

Figure 3 Etch pit density versus phosphorous ion dose for four different target temperatures during ion implantation. Diamonds: Target held at liquid nitrogen temperature; solid squares: room temperature; triangles: 150 °C; and circles: 300 °C.

To test the effect of target temperature on the threshold of secondary defect formation, a simple experiment was performed[4]. Phosphorous ions were implanted into Si wafers at energy of 200 keV. Some samples were held at room temperature while others were cooled to liquid-nitrogen temperature or heated to 150 or 300 °C during the ion implantation. Care was taken that all implantation were done at the same current density and with the same orientation of the crystal axes with respect to the ion beam (in order to avoid channeling effects). All samples received identical thermal anneals. Secondary defects, if any, were exposed by a defect sensitive chemical wet etch (Wright etch)[5] and the density of secondary defects was estimated by counting the etch pits on optical micrographs. Results of such counting exercises are shown in Figure 3, which shows the areal density of etch pits as a function of ion dose. The data points are grouped along four curves, corresponding to the four different ion implantation temperatures. It can be seen that the dose required to reach a certain number of etch pits per cm^2 increases with implantation temperature. Using an ad-hoc value of 10^{-4} etch pits per μm^2 as the threshold for secondary defect formation, it follows that the critical dose increases from 1×10^{14} ions/cm^2 for a room temperature implantation to 1.23×10^{14} ions/cm^2 at 150 °C and 1.63×10^{14} ions/cm^2 at 300 °C.

These initial results show that, indeed, the critical dose for secondary defect formation does appear to increase with the target temperature during the implantation. It would be interesting to further pursue these issues, for example what is the nature of the temperature dependence, how high in target temperature can one go and still have beneficial effects, and what are the electrical characteristics of the hot implanted samples.

4. PHOTOSENSITIVITY IN OPTICAL FIBERS

The core of the standard single-mode telecommunication optical fibers used in this study is located at a depth of 62.5 μm, a depth that can be reached by multi-MeV protons. It is expected that ion implantation of such ions directly into the core of a fiber would modify the fiber's photosensitivity, much in the same way that ion implantation modifies the photosensitivity of pure and Ge doped silica planar samples. 'Photosensitivity' means that the index of refraction can be permanently changed by illumination with ultra-violet light, so that for example a permanent refractive index grating can be written in the core of the fiber[6,7]. In spite of its importance as a technological advance (it can be employed in devices such as retro-reflecting Bragg gratings, mode converter gratings, etc.), photosensitivity is poorly understood. Germanosilicate fibers are known to be intrinsically photosensitive, and the purpose of the experiments described in this section is to establish the influence of proton implantation directly into the core of the fiber on its photosensitive properties. This could lead to improved understanding of the origin of photosensitivity as well as to the possibility of new or better devices.

Corning SMF-28 single-mode telecommunication fibers were used in the experiment described in this section. The core of the fiber has a diameter of 9 μm and is made of Ge-doped silica SiO_2:GeO_2, the concentration of GeO_2 being equal to 3 mole-%. The core is embedded in a cladding of pure silica with a diameter of 125 μm. Samples of the fiber have been implanted at room temperature with 1.4 MeV to 3.3 MeV protons. Several of the samples were implanted using an external beam. In this case protons exited the vacuum system through a thin Al window and passed through 10 cm of air before reaching the fiber. Other samples were implanted in a vacuum of ~10^{-7} torr.

Photographs of white light transmitted through the cross-sections of optical fibers implanted at different proton energies are shown in Figure 4. The bright circle at the center of each photograph corresponds to light guided by the core of the fiber. The luminous arc across the fiber corresponds to the region where the proton implantation induced an appreciable increase in the refractive index. This increase resulted in the formation of a waveguiding region under the implanted surface. The distance from the fiber surface to the induced waveguide is constant, as shown in Figure 4(b) by the dashed circle representing the offset fiber circumference, which is represented by the white circle. The most significant increase in the refractive index occurs at the end of proton range being centered at the same depth as the nuclear stopping region. This result is in agreement with the measurements of the profile of the refraction index in proton-implanted silica fibers[8].

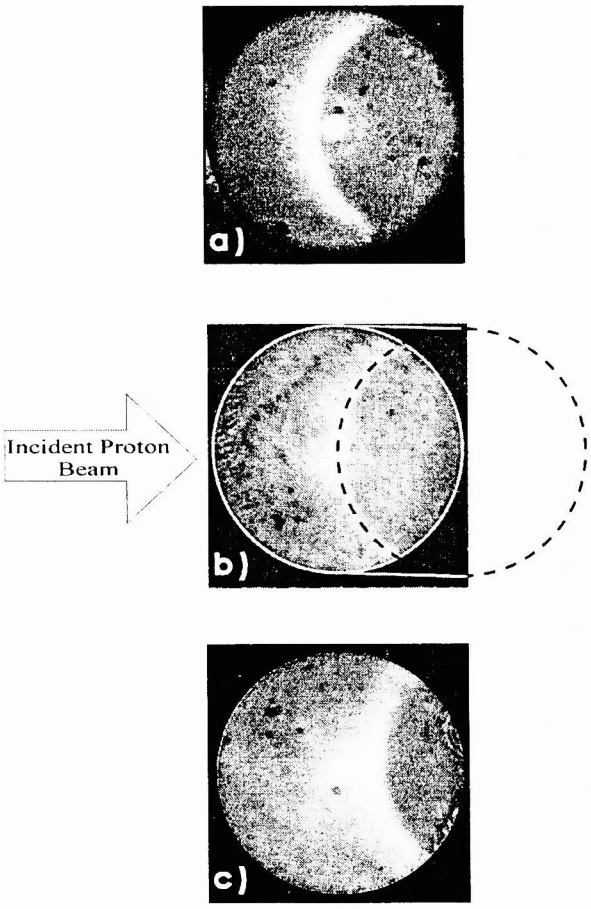

Figure 4. Photographs of light transmitted through implanted section of fibers showing guiding in the region of increased refractive index for different energies of protons incident on the fiber. a) E_{inc} =2.2MeV. Protons did not reach the core of the fiber. b) E_{inc} = 2.6MeV. Protons came to rest in the core of the fiber. c) E_{inc}=3.0MeV. Protons passed through the core of the fiber. The circles in Figure 4(b) are described in the text.

The photosensitivity of the implanted fibers has been examined by measuring the reflectivity of a Bragg grating written in the implanted section of fiber samples using the phase mask technique[9] and an ArF excimer laser (λ=193 nm, 100 pulses/sec, 0.35 J/cm^2/pulse). In all three samples the H^+ implantation in the core resulted in a decrease of the fiber's photosensitivity compared to that of unimplanted fiber exposed under the same conditions (see Figure 5 for the sample implanted at a fluence of $5{\cdot}10^{15}$ H^+/cm^2). Also, the initial Bragg grating central wavelength in the implanted fiber of Figure 3 is 1556.6 nm, longer by 1 nm than that of the unimplanted fiber. This indicates that implantation alone increased the refractive index in the core of the fiber by 0.001. Since this increase is likely not limited to the core but occurs everywhere near the proton end of range, this explains the waveguiding observed in Figure 4.

The implantation-induced photosensitivity is likely of opposite sign as the intrinsic photosensitivity in germano-silicate fibers. It was shown that in pure silica and implanted Ge-doped silica the ultraviolet induced index changes were negative and strongly correlated with bleaching of the implantation-induced absorption bands[10,11,12]. Since the net index change observed in our experiments is positive (this follows from the red shift of the Bragg grating wavelength), a small negative contribution to the UV-induced index change induced by the implantation would explain the observed net decrease in photosensitivity. Another possible contribution to the photosensitivity could be the chemical effect of the presence of hydrogen[13], even though the hydrogen concentrations in the present experiment are well below those required for photosensitivity induced by hydrogen loading.

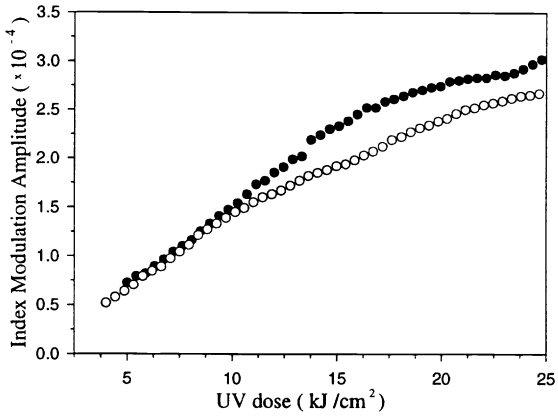

Figure 5. The rate of refraction index change versus UV irradiation time. The dashed line corresponds to an unimplanted sample and the full line corresponds to the sample implanted at $5{\times}10^{15}$ H^+/cm^2.

Concluding this section, we have demonstrated that protons can be accurately implanted through the cladding into the core of standard telecommunications fibers and that the optical properties of the fibers are modified as a result.

5. MAGNETORESISTANCE AND ION BEAM MIXING

Giant magnetoresistance[14] (GMR) is the phenomenon of large changes in the electrical resistivity, induced by a magnetic field. It has been observed in a variety of inhomogeneous materials such as some metallic multilayers and dispersions of clusters in a solid matrix. The interest in GMR stems from the enigma of its origin and from its obvious importance for possible applications such as disk drive read heads. It is believed that the structure of the interfaces between the constituents of the inhomogeneous samples plays a decisive role in GMR, and whence there is an interest in a study where this structure is systematically varied. The interfaces in a multilayer structure can be varied by carefully controlling the deposition parameters, but this is not a practical method for such a study, in part because for every new interface condition, a new sample has to be made. We have used ion beam mixing to modify the interface structure in existing multilayer samples. By increasing the ion fluence, the interfaces become increasingly blurred and any changes in the GMR of the samples is due to this blurring only, and neither to accompanying changes in crystallographic structure due to different deposition conditions nor to random sample-to-sample variations.

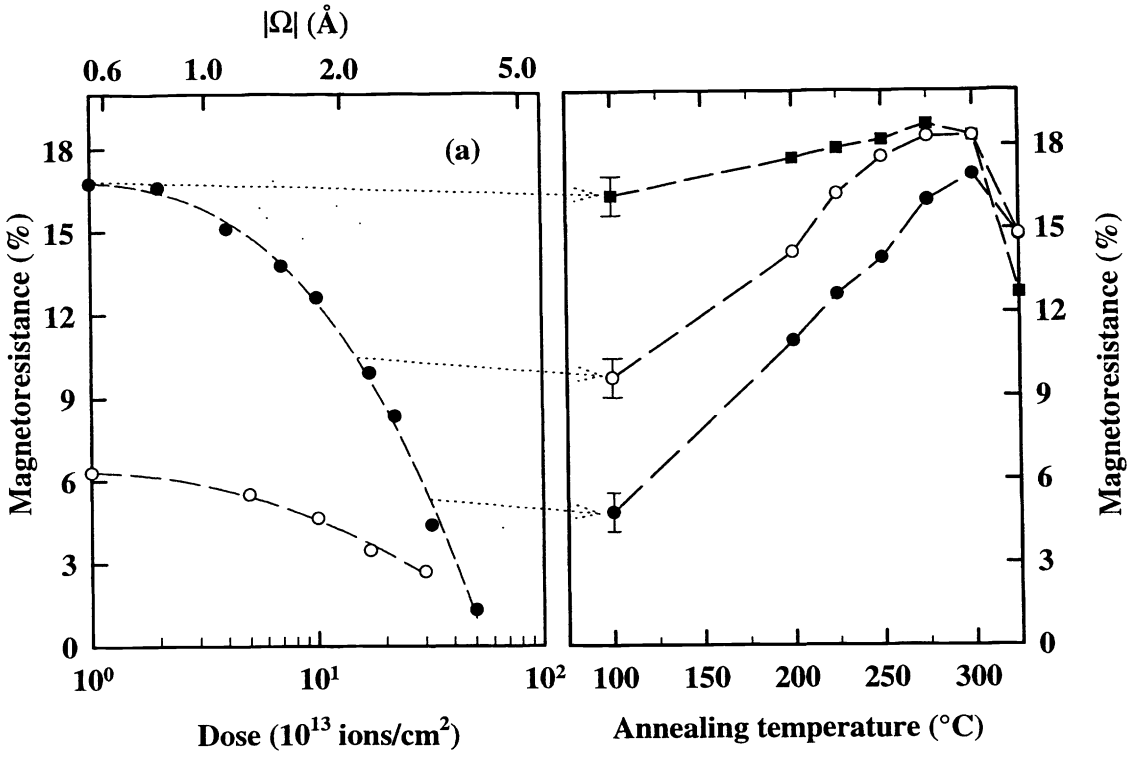

Figure 6 (Left panel): Magnetoresistance as a function of ion dose for a 30×[Co(17 Å)/Cu(22 Å)] (solid circles) and a 30×[Co(17 Å)/Cu(34 Å)] multilayer sample (open circles). The top scale gives the theoretical cascade mixing width. (Right panel): Variations in the GMR with annealing temperature for three 30×[Co(17 Å)/Cu(22 Å)] multilayer samples subjected to no implantation (solid squares), 1.3×10^{14} ions/cm^2 (open circles), or 2.6×10^{14} ions/cm^2 (solid circles).

Alternating Co (17 Å) and Cu (22 or 34 Å), repeated 30 times, were deposited by RF triode sputtering onto glass (Corning 7059) substrates. The deposition rates were 1 Å/s for Co and 2 Å/s for Cu. For a Cu interlayer thickness of 22 or 34 Å, the GMR oscillation is at a maximum. Surface profilometry and low-angle x-ray reflectivity measurements using Cu K_α radiation confirmed the thicknesses of the deposited layers. Ion beam mixing was performed with 1 MeV Si ions at current densities below 50 nA/cm^2, and with the samples cooled to liquid nitrogen temperature. Ion fluences ranged from 10^{12} to 5×10^{14} ions/cm^2. The depth penetration of 1 MeV Si is well beyond the total thickness of the deposited structure, so that very few ions came to rest in the actual multilayer. Collisions between the passing ions and target atoms displaced about 0.1 to 50 % of the atoms in the multilayer depending on the ion fluence, which leads to ion beam mixing at the interfaces. The damage profile throughout the multilayer is expected to be relatively uniform as the energy loss of the MeV ions shows little variation over its thickness. Some of the irradiated samples were vacuum annealed at temperatures up to 325 °C. A vibrating sample magnetometer was used to measure the room-temperature magnetization of the samples and a high-resolution AC bridge was used to determine the room-temperature magneto-transport properties.

X-ray reflectivity measurements (not shown here[15]) exhibited first and second order superlattice peaks, which indicated that the interfaces of the multi-layers are well defined. Ion irradiation reduced the amplitude of the peaks somewhat, indicative of interface intermixing, but even at the highest ion fluence the superlattice remained clearly intact. The full amplitude could be restored by thermal annealing. This is not unexpected since Cu and Co are immiscible, and it underlines how the interface structure can be varied while keeping the rest of the multilayer character intact by using ion beam mixing[16,17]. Detailed analysis of the x-ray reflectivity measurements through curve fitting showed that the interface mixing extended to 4 Å for the highest ion fluence.

Even at ion fluences where interface mixing was barely detectable by x-ray reflectivity, large changes in the magneto-transport properties could be observed. These are shown in figure 6. This figure has two panels, with the one on the left showing the reduction in magnetoresistance as the ion fluence is increased and the one on the right showing how thermal annealing can restore the magnetoresistance. From the left panel, it can be observed that the GMR falls monotonically with ion dose for both types of multilayer structures. Since other experiments on pure Cu and pure Co samples of similar thickness and which had received similar ion beam irradiation showed no such changes, the behaviour in the left panel is indicative of the large extent to which the GRM in these samples is controlled by interface structure. The panel on the right shows that the GMR can be restored by thermal annealing. For anneal temperatures of 300 °C and over, the GMR no longer increases and sharply falls off. Some of the increase in GMR is attributed to grain growth, as it occurs in all samples including the non-irradiated reference. The increase in GMR is however much larger in the irradiated samples, and since the increase occurs in tandem with an increase in the amplitude of the first and second order peaks in the x-ray reflectivity signal (not shown), it is concluded that the sharpness of the interface plays a major role in determining the GMR.

Interfacial mixing can affect the GMR in two principal ways: the introduction of additional electron scattering centers (with a spin-dependent scattering asymmetry different from other mechanisms) which would be a direct effect on the GMR; or the modification of the interlayer coupling, an indirect effect. The latter effect could come about indirectly or directly. Indirectly, if the mixed interfacial layer effectively adds to the thickness of the non-magnetic (Cu) spacer layers, at the expensive of the thickness of the magnetic (Co) layers. Or directly, through a suppression of the antiferromagnetic (AF) coupling due to strong disorder between Cu and down-spin Co states[18].

Concluding this section, ion beam irradiation of Co/Cu multilayer samples at low doses provides a means of intermixing and roughening interfaces between metallic layers of multilayer samples. The AF interlayer coupling and the GMR can be reversibly altered over a wide range, after the deposition of Co/Cu films, by using ion beam mixing and thermal annealing. It was found that the GMR is indeed strongly dependent on the interface sharpness and structure.

CONCLUSION

In conclusion, this paper described some of the activities around the new Tandetron accelerator aimed at studying the modifications in some electrical, optical, and magnetic materials. The threshold dose for secondary damage in Si was seen to increase with target temperature during ion implantation, as inferred from etch pit density following thermal anneal treatments of 200 keV P ion implanted Si samples. MeV protons have been implanted directly into the core of standard telecommunication optical fibers and modify the index of refraction at the end of their range. The photosensitivity of the core is reduced, likely because photosensitivity induced by the ion implantation is of opposite sign as the intrinsic photosensitivity. Intermixing of metallic multilayers can be probed by giant magnetoresistance, as is shown by the large reduction of magnetoresistance of Co/Cu multilayers upon irradiation with 1 MeV Si ions and the subsequent recovery by thermal anneal treatments.

ACKNOWLEDGMENTS

Many colleagues and students contributed in one way or another to the work described in this paper and it is a pleasure to acknowledge the contributions of J.L. Brebner, R.W. Cochrane, J. Albert (CRC), R. Abdouche and M. Sutton (McGill), and S. Chazal. It also is a pleasure to acknowledge the expert assistance of P. Bérichon and R. Gosselin with the operation of the tandem accelerator. This work is supported by the Natural Sciences and Engineering Research Council of Canada (NSERC) and by the Fonds pour la Formation de Chercheurs et l'Aide à la Recherche (FCAR).

REFERENCES

[1] See, for example, J.F. Ziegler, "*Ion Implantation Technology*", Ion Implantation Technology Co. (1996).
[2] K.S. Jones, S. Prussin, and E.R. Weber, Appl. Phys. **A45** (1988), 1, and references therein.
[3] R.J. Schreutelkamp, J.S. Custer, J.R. Liefting, W.X. Lu, and F.W. Saris, Mater. Sci. Rep. **6** (1991) 1.
[4] S. Chazal, F. Schiettekatte, and S. Roorda, *unpublished.*

[5] M. Wright Jenkins, J. Electrochem. Soc. May 1977, 757.
[6] K. O. Hill, Y. Fujii, D. C. Johnson, and B. S. Kawasaki, Appl. Phys. Lett. **32**, 647 (1978).
[7] H. G. Meltz, W. W. Morey, and W. H. Glenn, Opt. Lett. **14**, 823 (1989).
[8] H. M. Presby and W. L. Brown, Appl. Phys. Lett. **24**, 511 (1974).
[9] K. O. Hill, B. Malo, F. Bilodeau, D. C. Johnson, and J. Albert, Appl. Phys. Lett. **62**, 1035 (1993).
[10] J. Albert, B. Malo, K. O. Hill, D. C. Johnson, J. L. Brebner, and R. Leonelli, Opt. Lett. **17**, 1652 (1992).
[11] M. Verhaegen, J. L. Brebner, L. B. Allard, J. Albert, Appl. Phys. Lett. **68**, 3084 (1996).
[12] D. Kyle, B. L. Weiss, and G. D. Maxwell, J. Appl. Phys., **77**, 1207 (1995).
[13] P. J. Lemaire, R. M. Atkins, V. Mizrahi, and W. A. Reed, Electron. Lett. **29**, 1191 (1993).
[14] M.N. Baibich, J.M. Broto, A. Fert, F. Nguyen Van Dau, F. Petroff, P. Etienne, G. Creuzet, A. Friederich, and J. Chazelas, Phys. Rev. Lett. **61**, 2472 (1988).
[15] M. Cai, T. Veres, R.W. Cochrane, S. Roorda, R. Abdouche, and M. Sutton, in: "*Atomistic Mechanisms in Beam Synthesis and Irradiation of Materials*" Proc. Mater. Res. Soc. Symp. Vol. 504, Eds: J.C. Barbour, S. Roorda, and D. Ila, *in press.*
[16] M. Cai, T. Veres, S. Roorda, R.W. Cochrane, R. Abdouche, and M. Sutton, J. Appl. Phys., **81**, 5200 (1997).
[17] D.M. Kelly, I.K. Schuller, K. Korenivski, K.V. Rao, K.K. Larsen, J. Bottinger, E.M. Gyorgy, and R.B. van Dover, Phys. Rev. **B50**, 3481 (1994); K. Temst, G. Verbanck, R. Schad, G. Gladyszewski, and M. Hennion, Physica **B234-236**, 467 (1993).
[18] J. Kurnovsky, V. Drchal, I. Turek, M. Sob, and P. Weinberger, Phys. Rev. **B53**, (1996) 5125.